Journal of Polymer Research (2019) 26: 182
https://doi.org/10.1007/s10965-019-1848-8

ORIGINAL PAPER

Biodegradable dendrimer functionalized carbon nanotube-hybrids for biomedical applications

Sivaranjani Arumugam[1] · Padmapriya Ramamoorthy[2] · Lakshmi Devi Chakkarapani[3]

Received: 21 February 2019 / Accepted: 27 June 2019 / Published online: 6 July 2019

Abstract

In the present study, biodegradable poly(amidoamine) dendrimers (PAMAM G1/G2/G3) was covalently functionalized with carbon nanotubes (CNTs) and nanostructured hydroxyapatite was immobilized onto CNTs-PAMAM matrix through coordination bond between the $–NH_2$ groups of dendrimer and Ca^{2+} of hydroxyapatite. The structural and morphological behaviors of the nanohybrids were established through spectroscopic and microscopic analyses. In vitro cytotoxicity and cell proliferation was assessed through osteoblast-like MG 63 cell line using 3–4, 5-dimethylthiazole-2-yl, 2,5-diphenyl tetrazolium bromide assay for 3 days. The more abundant of $–NH_2$ group exist in PAMAM(G3) dendrimer attracts more number of HAp molecules onto their surface which exhibits enhanced activity in cell proliferations even at higher concentrations.

Keywords Carbon nanotubes · Dendrimer · Hydroxyapatite · Nanohybrids · Bone tissue engineering

Introduction

In recent years, combinations of nanotechnology and tissue engineering provides new horizon to nanostructured materials in biomedical applications. Specifically bone tissue engineering is an emerging filed due to numerous bone disorders, especially more than 20 million people are affected annually by accidents or diseases [1]. Some inorganic bioactive materials such as calcium phosphate, ceramics and bioactive glass, etc., have been applied for bone tissue engineering [2]. Hydroxyapatite (HAp) is a well-known calcium phosphate which belongs to apatite group. This HAp has the chemical formula of $Ca_{10}(PO_4)_6(OH)_2$ which resembles the inorganic component of bone and teeth. HAp is highly biocompatible biodegradable and osteoconductive material [3]. However, the brittle nature of inorganic bioactive materials cannot match with natural bone. Hence, it is not suitable for load bearing applications [4]. Under this circumstance, Carbon nanotubes (CNTs) have been chosen to improve the mechanical properties of hydroxyapatite.

Carbon nanotubes (CNTs) received greater interest in many research areas due to its excellent physical and chemical properties. Specifically, CNTs are widely used for biomedical applications such as tissue engineering, drug delivery, gene delivery, bone regeneration, biosensor, nano-pharmaceuticals, etc. [5, 6]. The remarkable properties of CNTs can provide mechanical, chemical and physical features for cell adhesion, proliferation and differentiation to form specific tissues. The different size and shape, thermal and electrical conductivity, elasticity, optical and biocompatible behaviors enhance the growth of different cells which makes CNTs a successful candidate in tissue engineering discipline [7, 8]. Even though CNTs is considered as a promising candidate for biomedical applications, it has poor dispersibility and processability. To overcome these issues, many researchers tried to modify CNTs surface by attaching hydrophilic polymers [9]. However, these

✉ Sivaranjani Arumugam
sivaranjaniarumugam88@gmail.com

[1] Department of Chemistry, Bharath Institute of Higher Education and Research, Chennai, Tamil Nadu 600 073, India

[2] Department of Pharmacology, JIPMER, Puducherry, India

[3] Laboratoire d'Electrochimie Physique et Analytique, Ecole Polytechnique Fédérale de Lausanne, Rue de l'Industrie 17, CH-1951 Sion, Switzerland

efforts were not enough to improve the hydrophilic nature of CNTs.

Therefore, dendrimers have been introduced by some researchers to improve the aqueous dispersibility of CNTs [10–13]. Dendrimers are highly branched and spherical shaped polymers. The unique properties of dendrimers viz., monodispersive, biocompatible and biodegradable nature, controllable molecular weight and highly reactive surface functional groups makes it a promising candidate in biomedical applications such as drug delivery, gene delivery, tissue engineering and biosensing [14, 15]. Recently, the combinations of dendrimers and carbon nanotubes have been widely used for biomedical applications due to its novel properties. Particularly, poly(amidoamine) (PAMAM) dendrimers have highly active hydrophilic terminal NH_2 functional groups. These NH_2 groups can be increased by increasing the generation of dendrimer. Further, the low toxicity and intrinsic biocompatibility of PAMAM makes it a best candidate for biomedical applications [3].

Considering these background, in this present study we have synthesized three different types of PAMAM dendrimer functionalized CNTs nanohybrids. Functionalization of dendrimer, CNTs and HAp deposition was investigated by Fourier Transform Infrared spectroscopy. Crystalline properties and particle size was confirmed by X-ray diffraction patterns. Morphologies and weight percentage of the elements present in nanohybrids were verified by Field Emission Scanning Electron Microscopy, High-resolution transmission electron microscope and Energy dispersive spectroscopy. Finally, the binding energy of

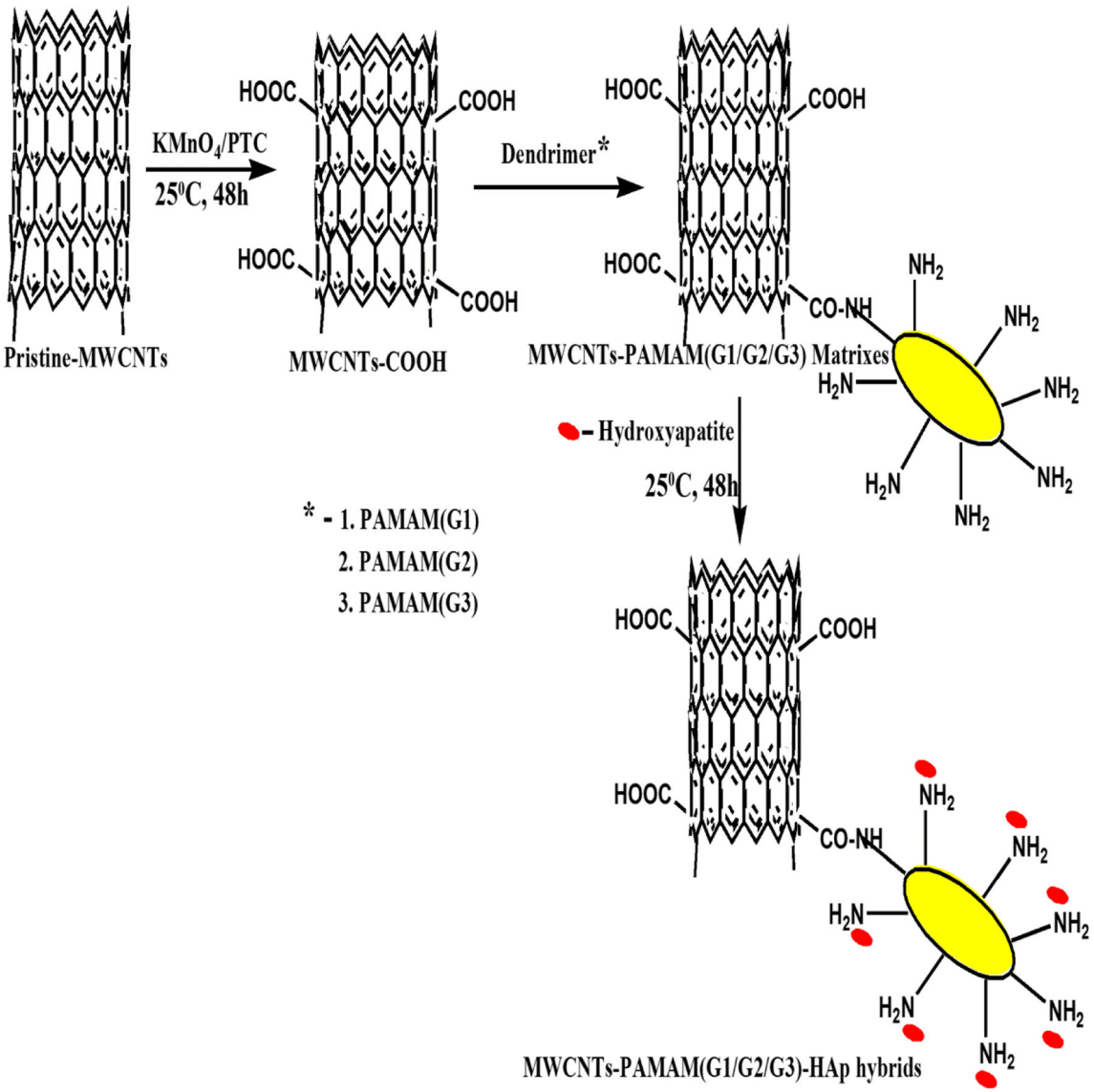

Fig. 1 Preparation of CNTs-dendrimer-hydroxyapatite nanohybrids

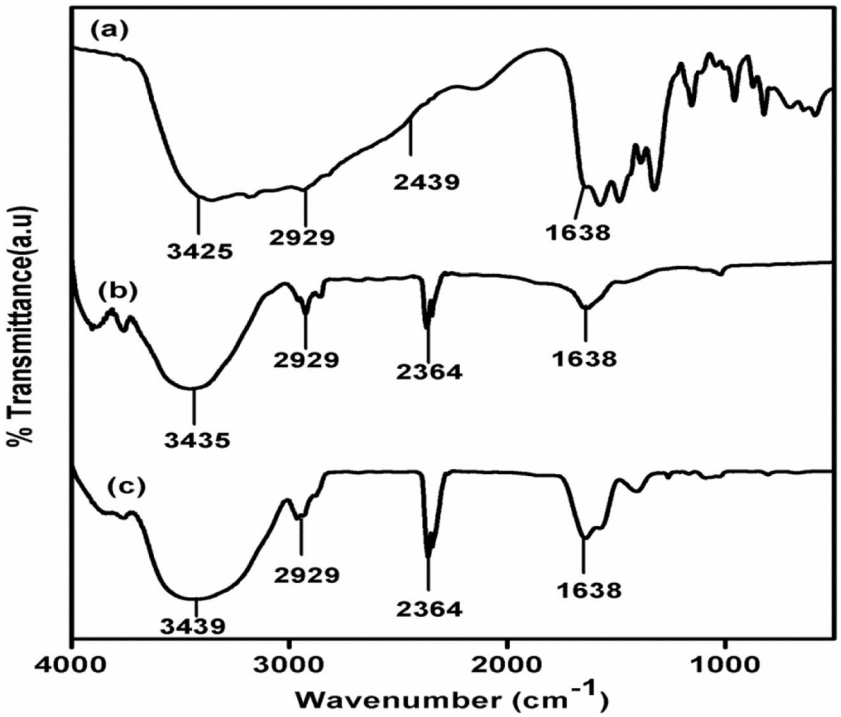

Fig. 2 FTIR spectra of (a) CNTs-PAMAM(G1), (b) CNTs-PAMAM(G2) and (c) CNTs-PAMAM(G3)

molecules and oxidation state was confirmed by X-ray photoelectron spectroscopy. In vitro cytotoxicity and cell proliferation was examined on osteoblast-like MG 63 cell line using MTT (3–4, 5-dimethylthiazole-2-yl, 2,5-diphenyl tetrazolium bromide) assay. The percentage of cell viability was monitored for 3 days and the obtained results showed the excellent activity of the newly synthesized nanohybrids.

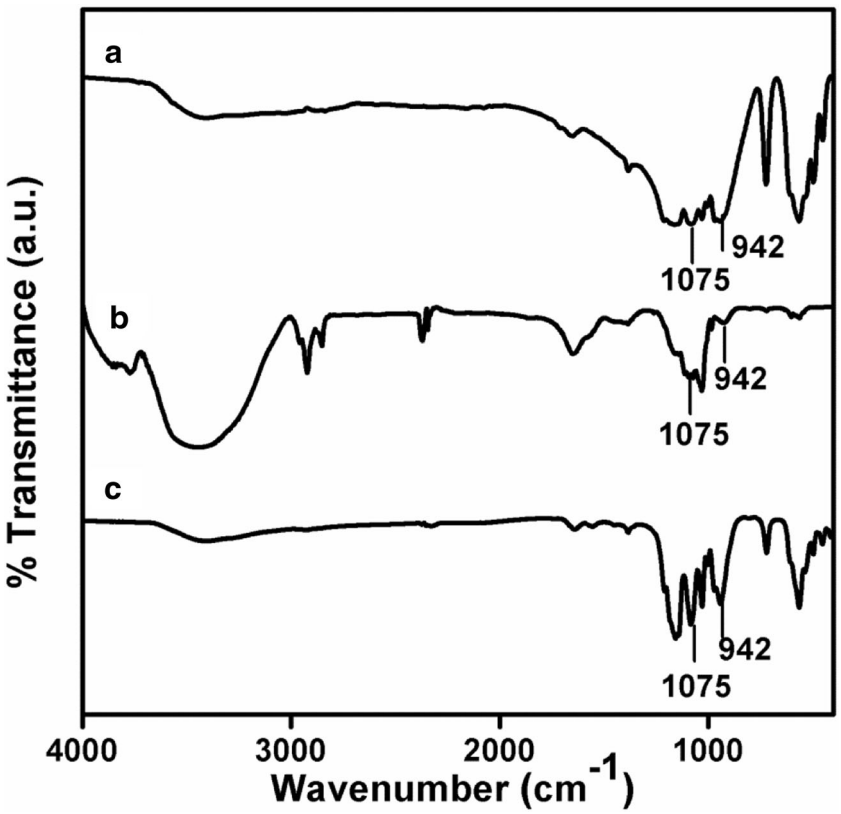

Fig. 3 FTIR spectra of (a) CNTs-PAMAM(G1)-HAp, (b) CNTs-PAMAM(G2)-HAp and (c) CNTs-PAMAM(G3)-HAp

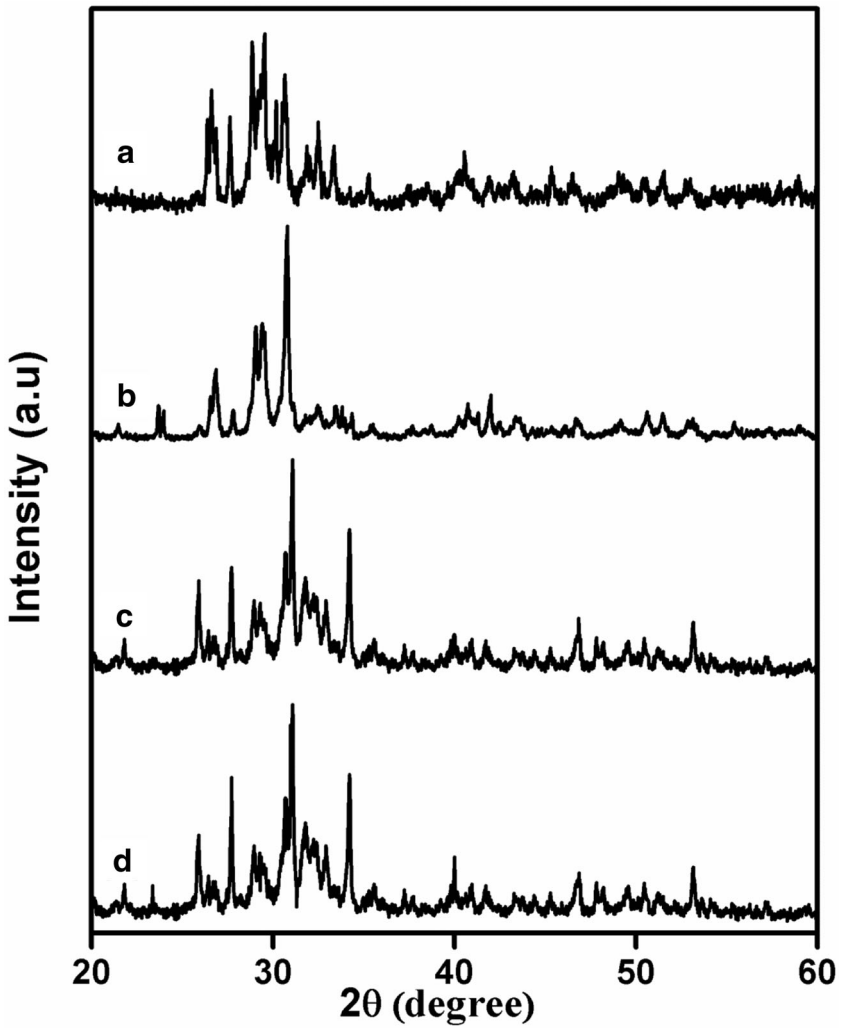

Fig. 4 XRD patterns of (a) HAp, (b) CNTs-PAMAM(G1)-HAp, (c) CNTs-PAMAM(G2)-HAp and (d) CNTs-PAMAM(G3)-HAp

Experimental methods

Preparation of CNT-COOH and hydroxyapatite

Initially acid group functionalized CNTs (CNTs-COOH) have been prepared by preheating the as-received CNTs (multi-walled carbon nanotubes with length and diameter of 10–30 μm and 50 nm and purity of 95%) at 350 °C for 2 h and then 50 mg of preheated CNTs were dispersed with dichloromethane (15 mL) for 10 min. Later, tetrabutyl ammonium bromide (0.25 g), acetic acid (5 mL) and $KMnO_4$ (0.065 g) were added to the above mixture and stirred vigorously for 48 h under ambient temperature. The resultant CNTs-COOH were centrifuged and washed with distilled water and then dried under vacuum [16, 17].

In a separate procedure hydroxyapatite has been prepared by adopting wet precipitation method. First, calcium nitrate tetrahydrate (40 mL of 0.32 M) was taken in a 250 mL round bottom flask, to which 2.5 mL of ammonia solution was added under stirring condition and the pH of the solution was maintained at 9. Later, 60 mL of potassium dihydrogen phosphate

Table 1 Results obtained from EDS, XRD and FESEM analyses

Name of the hybrids	Weight percentage of elements					Average Particle Size of HAp	
	C	N	O	Ca	P	XRD	FESEM
CNTs-PAMAM(G1)-HAp	23.30	3.41	39.88	18.50	11.91	24	25
CNTs-PAMAM(G2)-HAp	14.93	5.98	42.54	22.39	14.16	22	22
CNTs-PAMAM(G3)-HAp	3.12	8.24	45.52	25.18	17.94	19	16

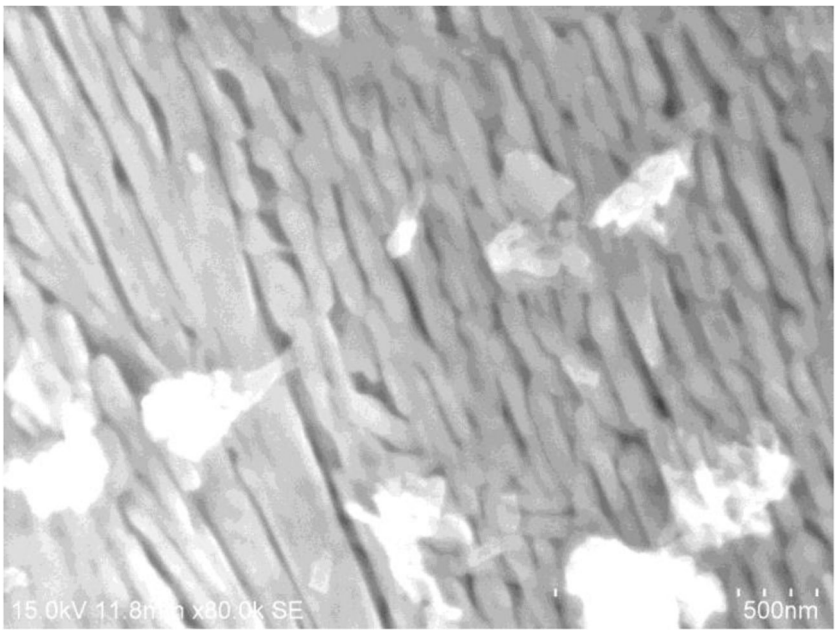

Fig. 5 FESEM of Hydroxyapatite

(0.19 M) was slowly added to the above mixture and which produce white precipitate [18, 19]. Then the mixture was stirred for 1 h under ambient temperature. The resultant was washed with water and centrifuged. The obtained residue was taken in a ceramic boat and thermally heated for 2 h at 400 °C and which produced synthetic hydroxyapatite (HAp) with the Ca/P ratio of 1.67 which mimics the extracellular matrix of bone [20].

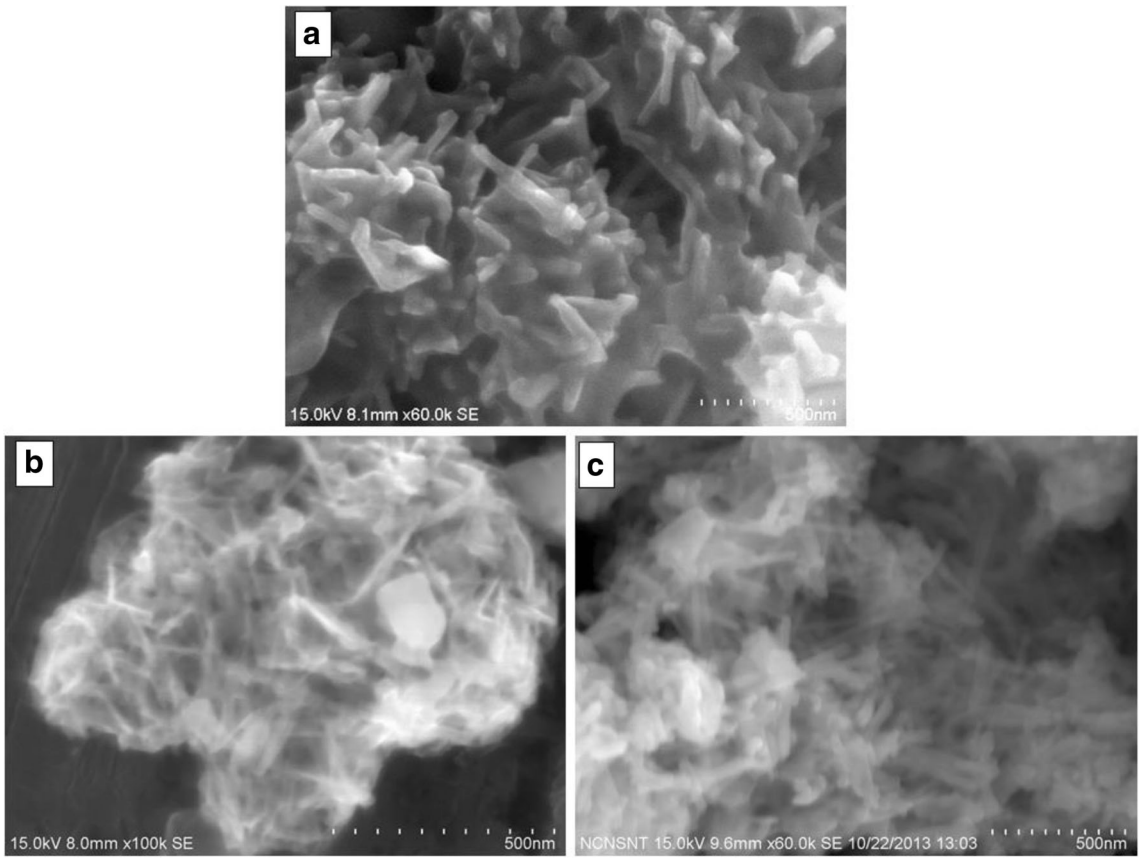

Fig. 6 FESEM of (a) CNTs-PAMAM(G1)-HAp, (b) CNTs-PAMAM(G2)-HAp and (c) CNTs-PAMAM(G3)-HAp

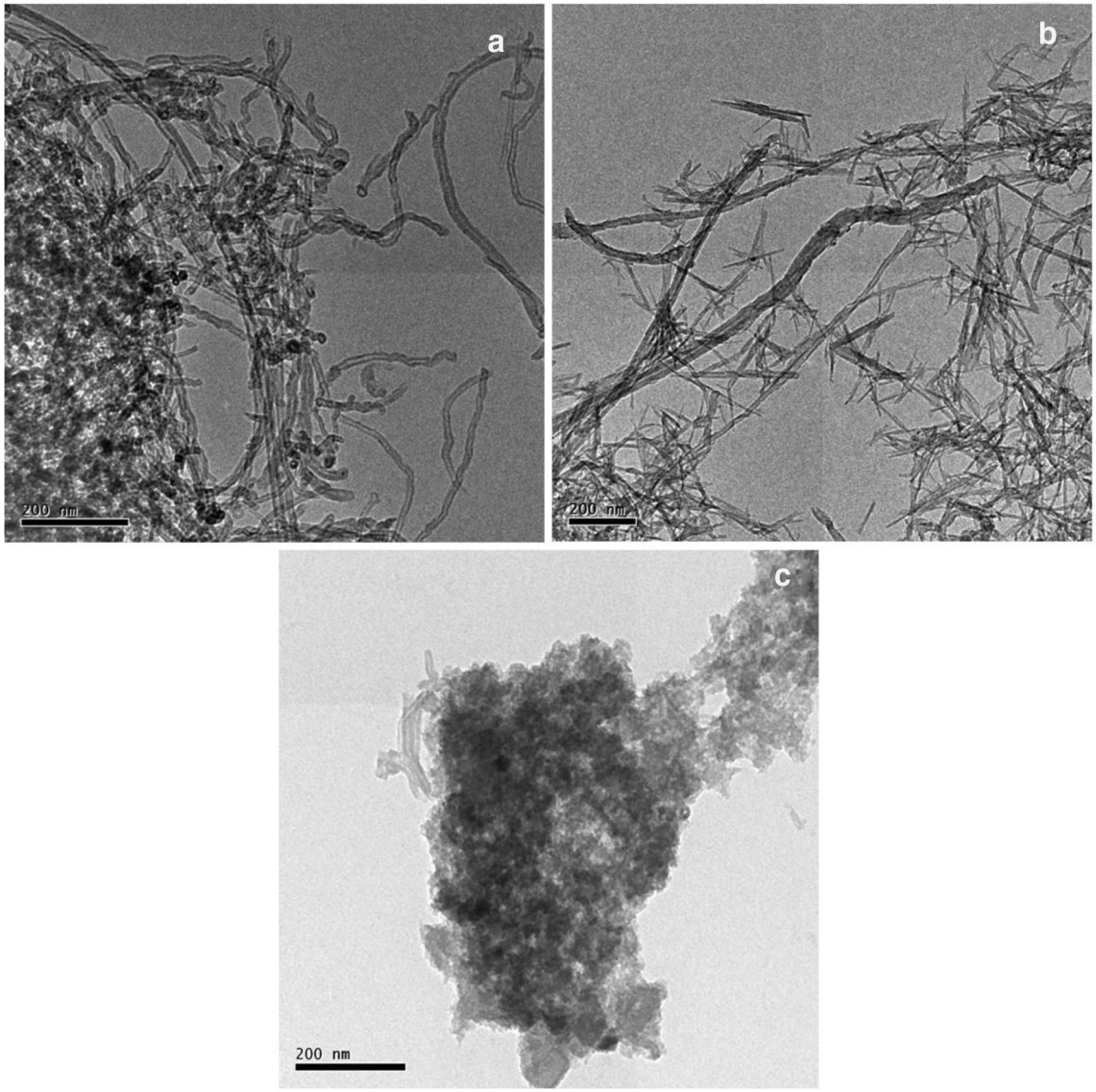

Fig. 7 HRTEM images of (a) Pristine-CNTs (b) CNTs-COOH and (c) nanostructured HAp

Synthesis of CNTs-dendimer matrixes

Synthesis of poly(amidoamine) dendrimer onto CNTs surface was carried out by adopting two different reaction mechanism viz., (1) Michael addition of methyl acrylate (MA) to peripheral amino groups and (2) amidation of terminal ester groups by ethylenediamine (EDA). First, acid functionalized CNTs (50 mg) were dispersed with 50 mL of distilled water for 10 min, to which 100 mg of 1-(3-dimethyl-amino-propyl)-3-ethyl carbodimide and N-hydroxy succinimide were added. Then, 100 mg of ethylenediamine was added to the above mixture and stirred vigorously under N_2 atmosphere at 60 °C for 24 h. The resultant product was washed with water and dried under vacuum and thus produced CNTs-G0-NH_2.

Then, Michael addition of MA to peripheral amino groups was carried out by taking 0.40 g of CNTs-G0-NH_2 in 250 mL RB flask and dispersed in 20 mL of methanol and to which 40 mL of methanol/MA solution (1:1) was added and the reaction was performed at 30 °C for 48 h. The resultant product was filtered, washed and dried, and thus yielded functionalized CNTs containing the "first generation" ester group which labeled as CNTs-G0.5-$COOCH_3$. The amidation of the terminal groups of CNTs-G0.5-$COOCH_3$ was carried out by dispersing 0.40 g of CNTs-G0.5-$COOCH_3$ with 20 mL of methanol in 250 mL RB flask and then 40 mL of methanol/EDA solution (1:1) was added to react at 30 °C for 48 h. The resultant was washed and dried to obtain functionalized CNTs containing "first generation" amino groups namely CNTs-G1-NH_2.

Similarly, the propagation to higher generations was carried out by repeating Michael addition of MA to amino groups and amidation of terminal ester groups with EDA. With a view to generate the second and third generation dendrimer, the

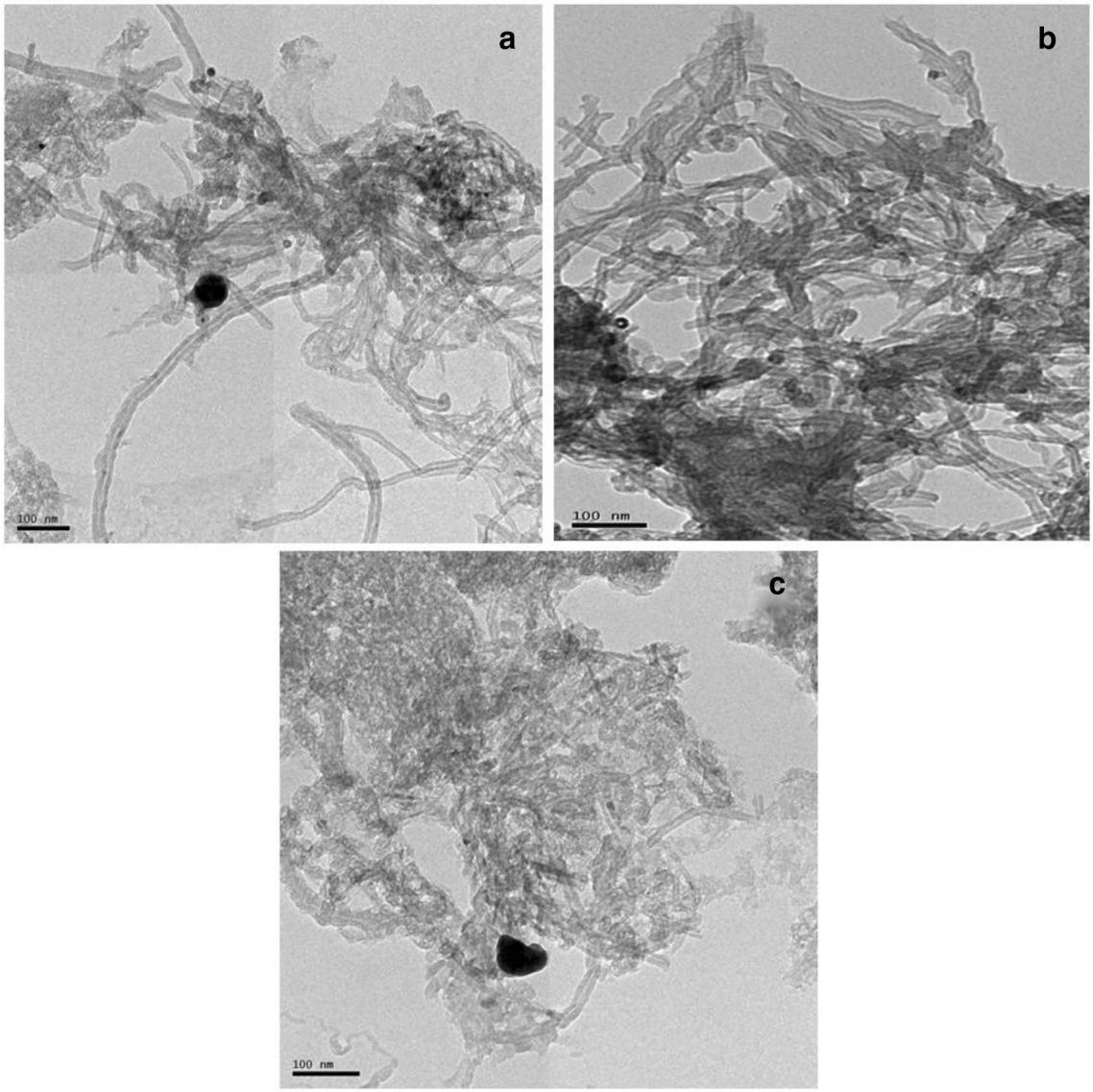

Fig. 8 HRTEM images of (a) CNTs-PAMAM(G1), (b) CNTs-PAMAM(G2) and (c) CNTs-PAMAM(G3)

CNTs-PAMAM(G1) matrix were employed again individually for Michael addition and amidation reactions by repeating the same experimental procedure with the quantum of same chemicals and thus yielded the corresponding matrixes viz., CNTs-PAMAM(G2) and CNTs-PAMAM(G3).

Synthesis of CNTs-dendrimer-HAp nanohybrids

Schematic illustration for nanohybrids formation was shown in Fig. 1. At first, 1.05 g of synthesized HAp was dispersed with 10 mL of distilled water, to which CNTs-PAMAM(G1) (5 mL, 0.24 g) and methanol (10 mL) were added drop-wise and then stirred for 48 h under room temperature. Then the resultant CNTs-PAMAM(G1)-HAp was lyophilized at −40 °C and dried by using air oven. Subsequently, by adopting the same experimental procedure and quantum of same chemicals, the CNTs-PAMAM(G2)-HAp and CNTs-PAMAM(G3)-HAp hybrids were also prepared individually by using CNTs-PAMAM(G2) and CNTs-PAMAM(G3) matrixes.

Characterizations

Structure and morphologies of the prepared samples were characterized by various spectroscopic and microscopic analyses. Fourier Transform Infrared spectra (FTIR) were performed by Bruker Tensor-27 FTIR spectrophotometer. Then X-ray diffraction patterns were obtained from Bruker D8 Advance X-ray diffraction. Field Emission Scanning Electron Microscopic (FESEM) images were taken by SU6600 HITACHI at 100 kV. Energy dispersive spectroscopy (EDS) was performed through EDS DX-4 combined with FESEM. High-resolution transmission electron microscopic

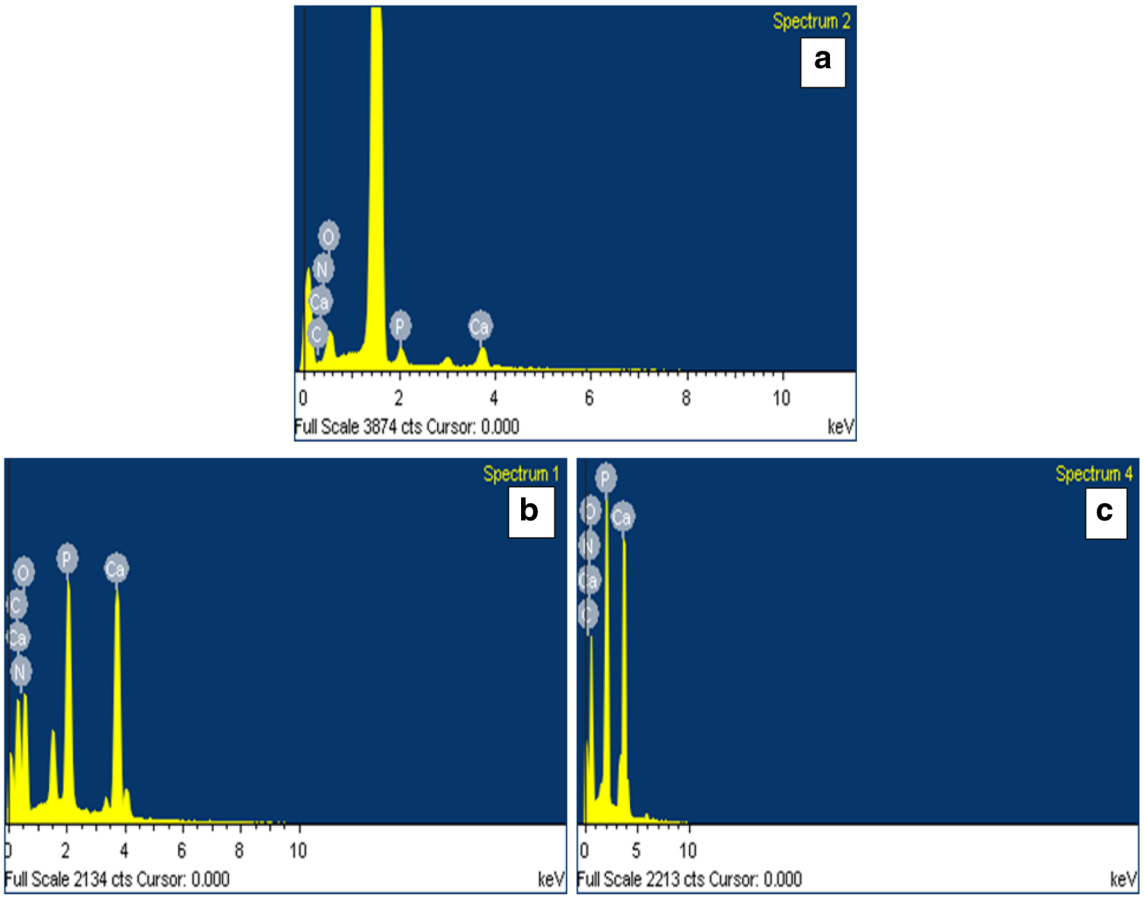

Fig. 9 EDS of (a) CNTs-PAMAM(G1)-HAp, (b) CNTs-PAMAM(G2)-HAp and (c) CNTs-PAMAM(G3)-HAp

(HRTEM) images were taken by JEOL 3010 at 300 keV. Finally, X-ray photoelectron spectra (XPS) was taken by UHV chamber of a photoelectron spectrometer, Omicron nanotechnology, Germany (GmbH) equipped with monochromatic X-ray source (AIKR h =1486.6 eV) and operated at15 kV and 20 mA (300 W).

Result and discussions

Structural and morphological characterizations

FTIR spectra of CNTs-PAMAM(G1), CNTs-PAMAM(G2) and CNTs-PAMAM(G3) matrixes and the corresponding nanohybrids are shown in Fig. 2a-c and 3a-c, respectively. CNTs-PAMAM(G1) exhibits the characteristic peaks at 1638, 2439 and 2929 cm^{-1} due to -CO-NH-, $C\text{-}H_{(str)}$ combination and CH_2 asymmetric stretching, respectively. Then the N-H asymmetric stretching was appeared at 3425 cm^{-1} and its broadening is due to hydrogen bonding (Fig. 2a). Similarly, CNTs-PAMAM(G2) showed the peaks at 1638 cm^{-1} for -CO-NH-, 2364 cm^{-1} for combination of $C\text{-}H_{(str)}$, 2929 and 2856 cm^{-1} for CH_2 asymmetric and symmetric stretching and 3435 cm^{-1} for N–H asymmetric stretching (Fig. 2b). Further, CNTs-PAMAM(G3) showed the characteristic peaks at 1638, 2364, 2929 and 3439 cm^{-1} corresponds to -CO-NH-, combination of $C\text{-}H_{(str)}$, CH_2 asymmetric stretching and N–H asymmetric stretching, respectively (Fig. 2c). The FTIR spectra of CNTs-PAMAM(G1)-HAp (Fig. 3a), CNTs-PAMAM(G2)-HAp (Fig. 3b) and CNTs-PAMAM(G3)-HAp (Fig. 3c) showed the characteristic peaks for hydroxyapatite at 1075 and 942 cm^{-1} corresponding to υ_3 mode of PO_4^{3-} asymmetric stretching and υ_1 mode of symmetric stretching, respectively [21]. Hence, the amide linkage from FTIR results supports the covalent bond formation between CNTs-COOH and PAMAM dendrimer, in addition, the appearance of characteristic peaks for HAp indicates the deposition of HAp onto CNTs-PAMAM matrixes [22].

The XRD patterns of synthesized HAp and three different types of CNTs-dendrimer nanohybrids are shown in Fig. 4a-d. The characteristic 2 peaks observed at 26.9°, 30.8°, 32.4°, 34.2°, 39.9°, 46.8° and 49.5° for HAp, CNTs-PAMAM(G1)-HAp, CNTs-PAMAM(G2)-HAp and CNTs-PAMAM(G3)-HAp were corresponding to (002), (211), (300), (202), (310), (222) and (213). These planes are belongs to hydroxyapatite with JCPDS data base

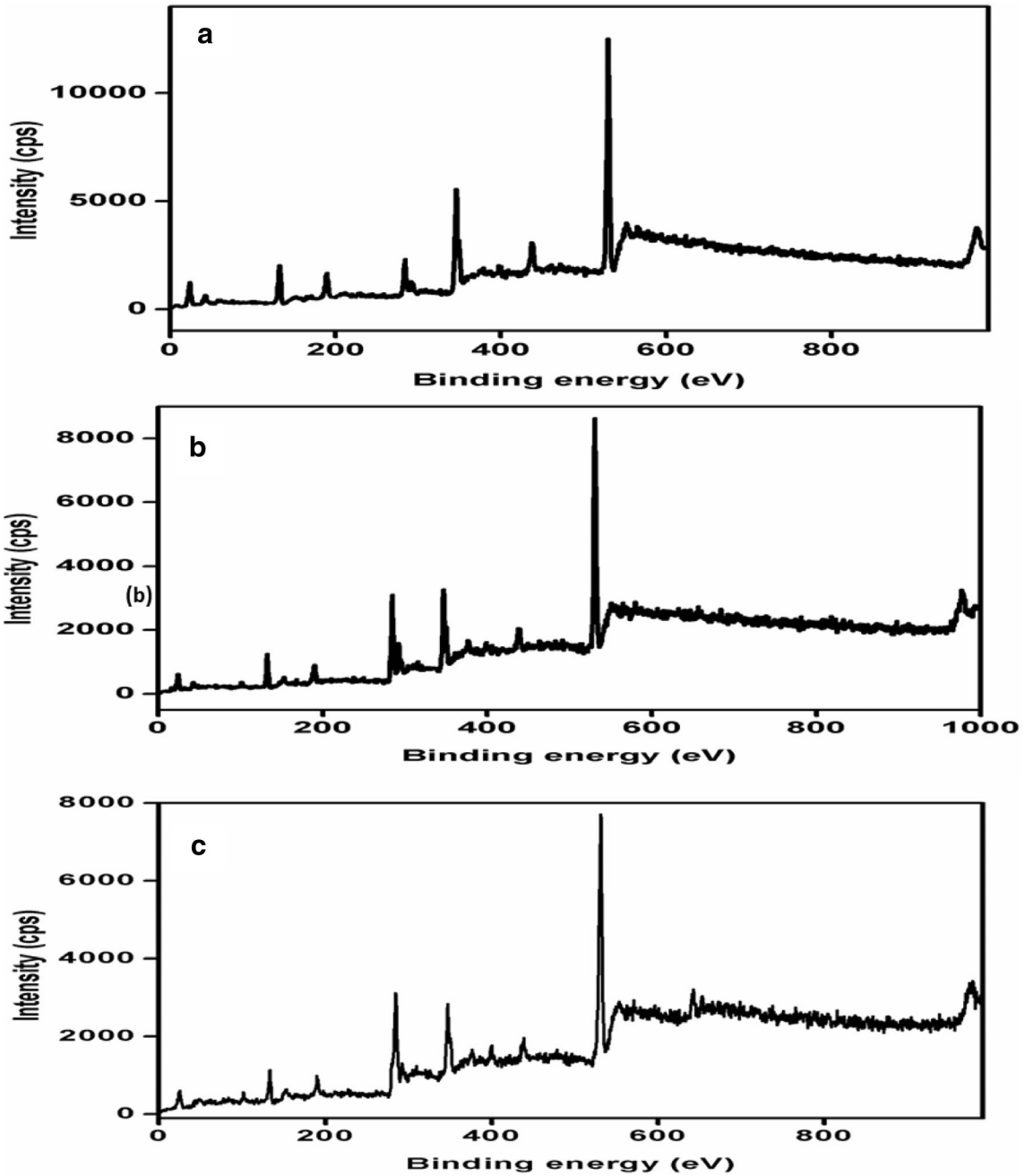

Fig. 10 XPS survey spectrum of (a) CNTs-PAMAM(G1)-HAp (b) CNTs-PAMAM(G2)-HAp (c) CNTs-PAMAM(G3)-HAp

number of 9–432. Hence, the obtained results confirmed the deposition of hydroxyapatite on CNTs-dendrimer matrixes. Further, (002) reflection was used to measure the crystalline size of the hydroxyapatite [23]. The calculated crystal size of the deposited HAp on CNTs-PAMAM(G1), CNTs-PAMAM(G2) and CNTs-PAMAM(G3) matrixes was found as 24, 22 and 19 nm, respectively (Table 1). The crystalline size of the HAp particle was decreased on increase in dendrimer generation number. This is due to the fact that the dendrimers with higher generations have increased numbers of surface amino groups which create more sites for complex formation and effectively helps to protect colloid formation [24].

The surface morphology of the nanohybrids was investigated by FESEM analysis. Figure 5 shows the traditional needle-like morphology of hydroxyapatite. The FESEM images of all the nanohybrids showed uniform distribution of white patches covered over CNTs-surfaces which indicates the deposition of HAp particles onto the respective matrixes (Fig. 6a-c). On comparing the images, CNTs-PAMAM(G3) matrix showed more quantum of white patches due to the abundance of more number of $–NH_2$ groups to capture more

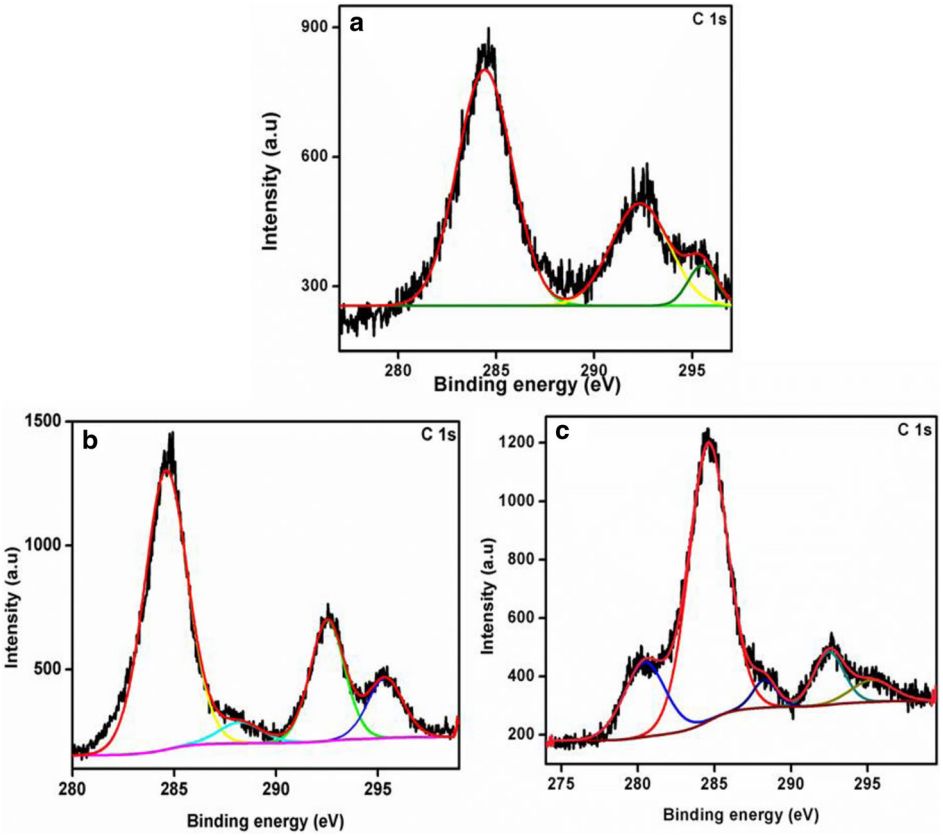

Fig. 11 XPS for C 1s of (a) CNTs-PAMAM(G1)-HAp, (b) CNTs-PAMAM(G2)-HAp and (c) CNTs-PAMAM(G3)-HAp

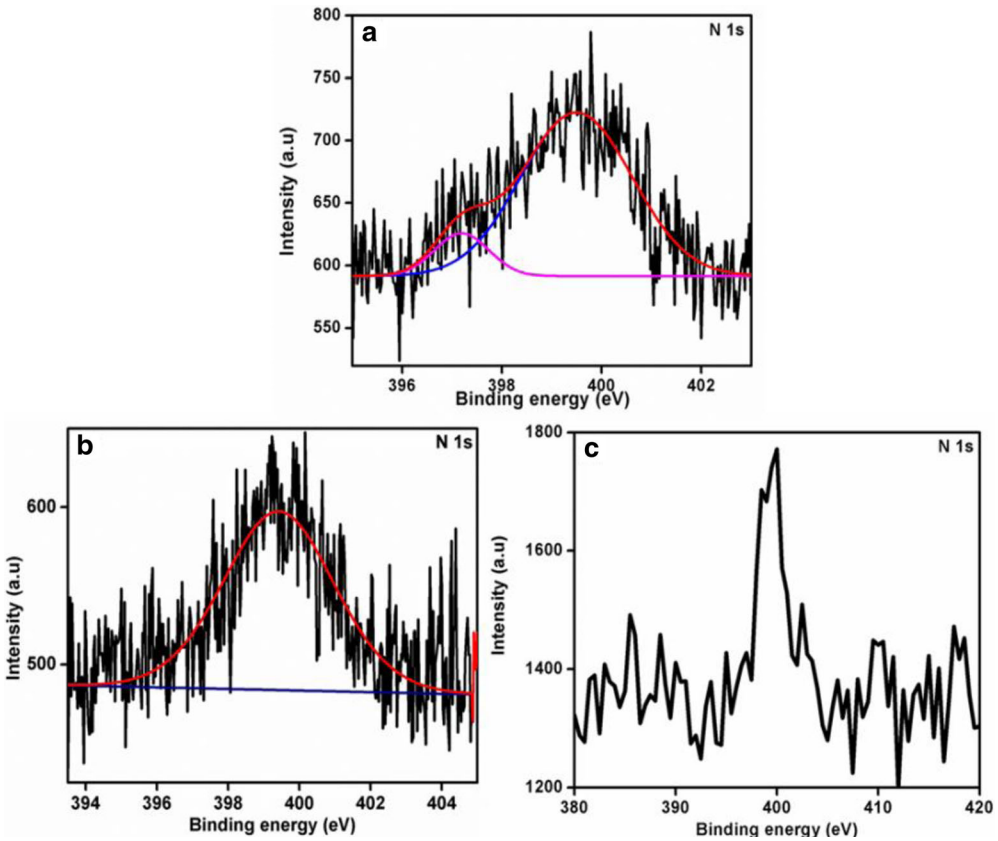

Fig. 12 XPS for N 1s of (a) CNTs-PAMAM(G1)-HAp, (b) CNTs-PAMAM(G2)-HAp and (c) CNTs-PAMAM(G3)-HAp

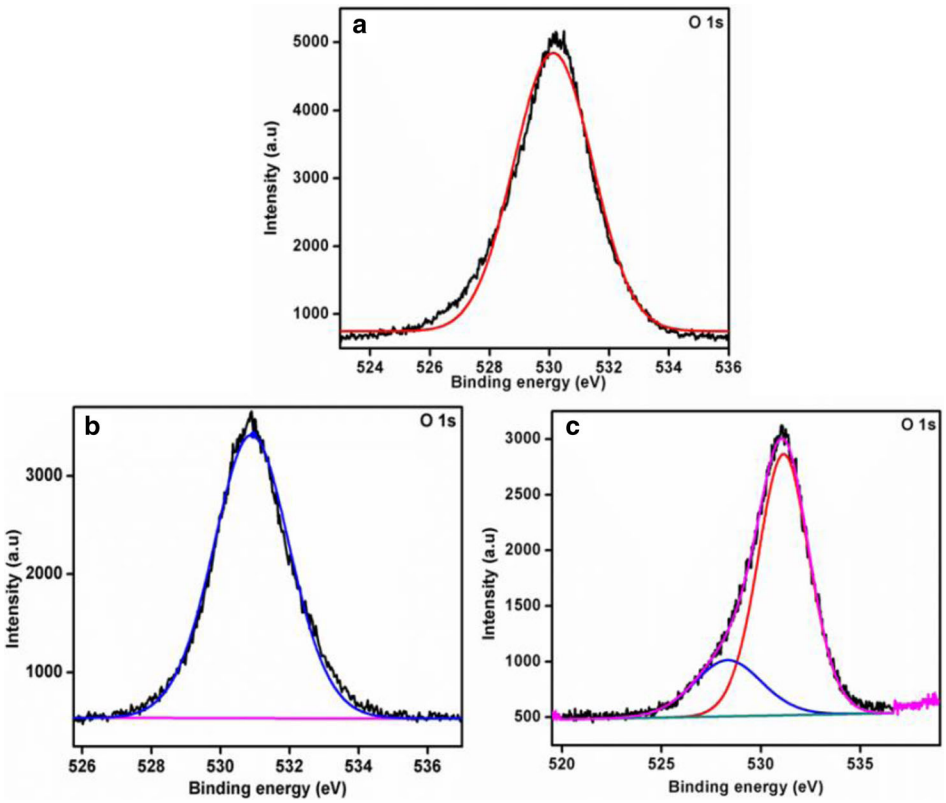

Fig. 13 XPS for O 1s of (a) CNTs-PAMAM(G1)-HAp, (b) CNTs-PAMAM(G2)-HAp and (c) CNTs-PAMAM(G3)-HAp

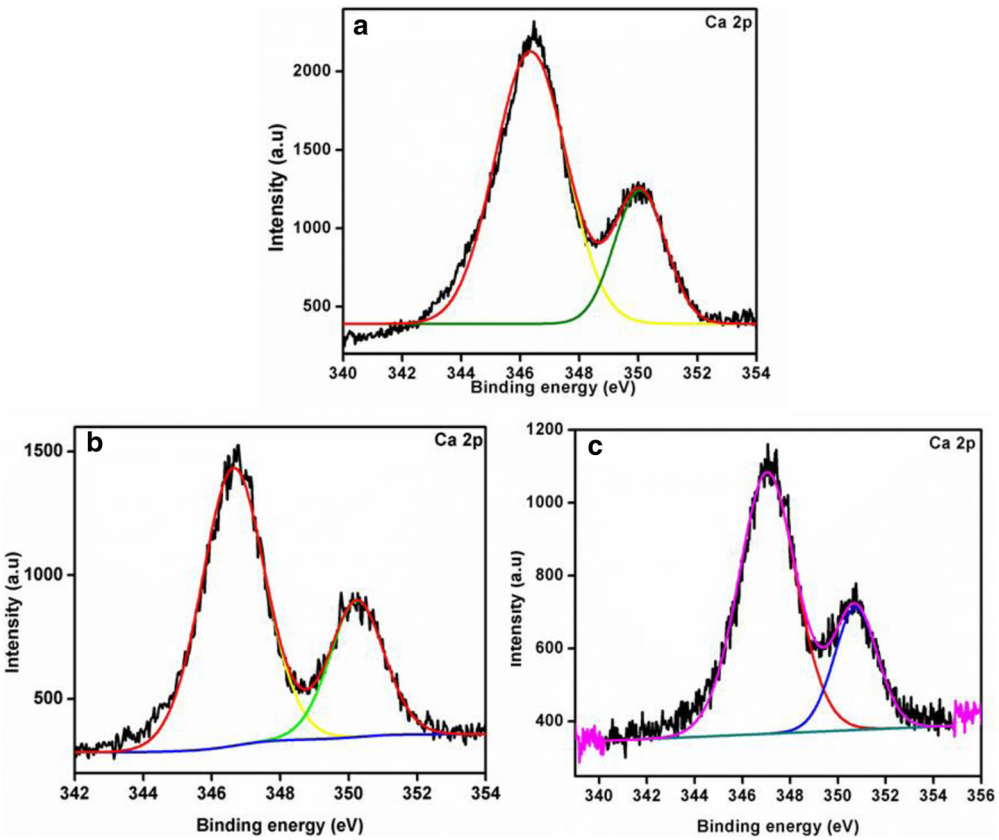

Fig. 14 XPS for Ca 2p of (a) CNTs-PAMAM(G1)-HAp, (b) CNTs-PAMAM(G2)-HAp and (c) CNTs-PAMAM(G3)-HAp

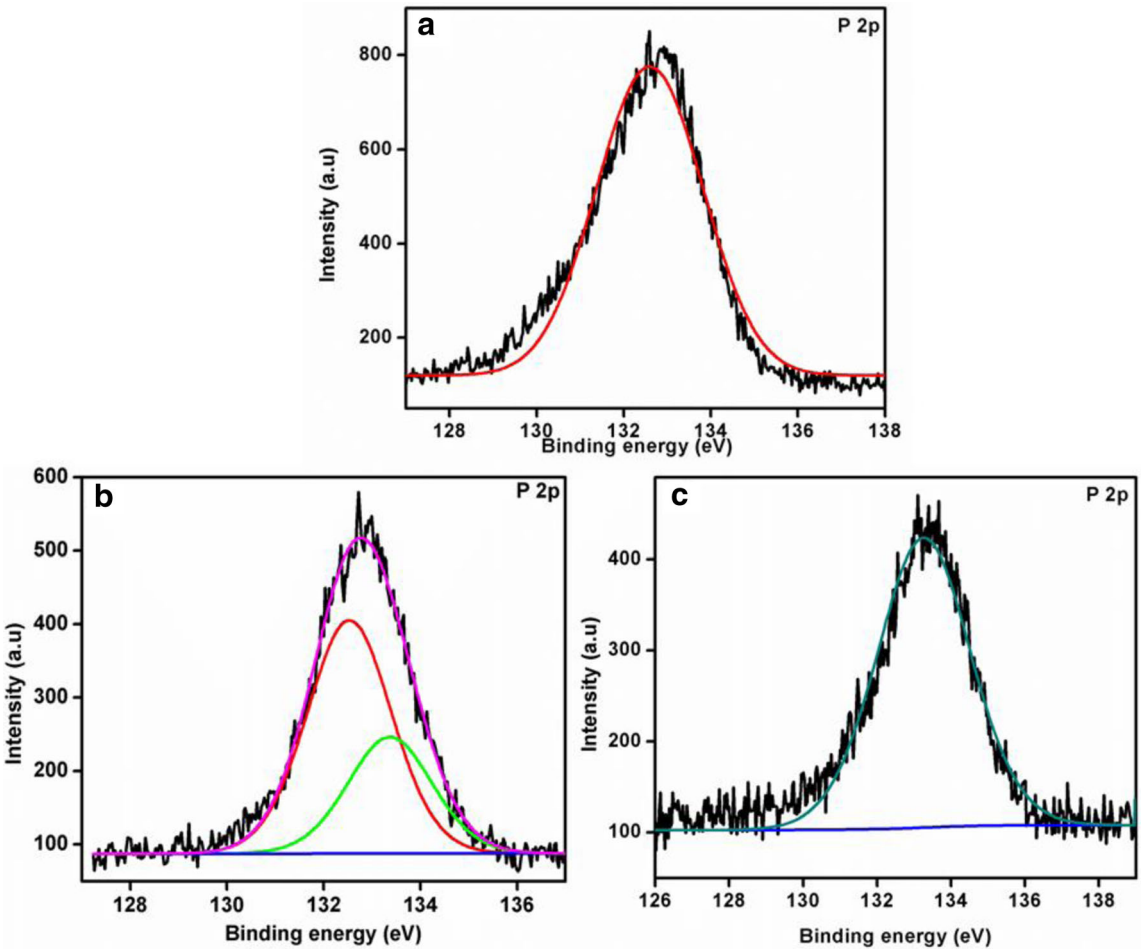

Fig. 15 XPS for P 2p of (a) CNTs-PAMAM(G1)-HAp, (b) CNTs-PAMAM(G2)-HAp and (c) CNTs-PAMAM(G3)-HAp

quantum of HAp molecules than other matrixes as discussed in XRD analysis. The morphologies of CNTs, HAp and PAMAM-modified CNTs were investigated by HRTEM analysis. In Fig. 7a, pristine-CNTs showed smooth and bundled structures. Whereas, in Fig. 7b, debundle structure of CNTs indicates the acid functionalization of CNTs and Fig. 7c shows the aggregated structures of hydroxyapatite nanocrystals. Further, the roughness/heterogeneity on tube surface (CNTs surface) was increased from CNTs-PAMAM(G1) to CNTs-PAMAM(G2) as shown in Fig. 8a-c. This surface heterogeneity indicates the covalent functionalization of dendrimer molecules onto CNTs surface. The weight percentages of the elements present in all the three nanohybrids were investigated by EDS analysis (Fig. 9a-c). Specifically, the weight percentage of Ca was found as 18.50, 22.39 and 25.18% in CNTs-PAMAM(G1)-HAp, CNTs-PAMAM(G2)-HAp and CNTs-PAMAM(G3)-HAp, respectively, whereas, the weight percentage of P was found as 11.91, 14.16, 17.94%. On comparing these results CNTs-PAMAM(G3)-HAp showed more weight percentage of Ca and P deposition than others which strongly supported the results obtained from FESEM analysis [25].

The binding nature of molecules in the formation of nanohybrids and oxidation states of Ca and P in HAp was investigated by XPS analysis. Figure 10a-c shows the XPS survey spectrum of CNTs-dendrimer nanohybrids which indicates the appearance of characteristic peak for C 1s, O 1s, N 1s, Ca 2p and P 2p. The deconvoluted C 1s (Fig. 11) peaks for CNTs-PAMAM(G1)-HAp was obtained at 284.42 and 292.34 eV, CNTs-PAMAM(G2)-HAp at 284.6, 288.11 and 292.52 eV and for CNTs-PAMAM(G3)-HAp at 284.54, 288.35 and 292.55 eV which are due to –C*–C–, C*-N and –C* = O bonds, respectively. The N 1s spectra (Fig. 12) showed the peaks around 397.2 and 399.98 eV are corresponding to the existence of $–NH_2$ and –NH groups in PAMAM. Then the O 1s (Fig. 13) showed the peak around 530.9 eV was due to –P–O*– which indicates the existence of PO_4^{3-} in HAp [26]. Ca 2p (Fig. 14) showed the peaks at 350.23 and 346.66 due to $2p_1$ and $2p_3$ of Ca 2p in HAp, respectively. Finally, P 2p (Fig. 15) showed the peak at 132.59 eV for P $2p_1$. The appearance of Ca 2p and P 2p peaks proved the oxidation state of Ca^{2+} and P^{5+} in HAp ($Ca_{10}(PO_4)_6(OH)_2$) [27–29].

In vitro cytotoxicity and cell proliferation assay

In vitro cytotoxicity of the newly synthesized nanohybrids were examined on osteoblast-like MG 63 cell line (obtained from NCCS, Pune, India) using MTT (3–4, 5-dimethylthiazole-2-yl, 2,5-diphenyl tetrazolium bromide) assay [18, 30]. In briefly, about 10,000 cells per well were seeded on 96 well plates and different concentrations of nanohybrids viz., 7.8, 15.6, 31.2, 62.5, 125, 250, 500 and 1000 μg/mL was treated for 24 to 72 h. Results were obtained from repeating the experiment for two times and the percentage of cell death was also assessed. Further, the morphological assessment of cells were performed using osteoblast-like MG 63 cells i.e. cell lines were treated with 31.2, 62.5, 125 and 1000 μg/mL concentrations of nanohybrids followed by incubation for 24 h. After the incubation period, morphological changes were analyzed under optical microscopy.

The percentages of cell viability of all the CNTs-dendrimer nanohybrids were plotted against with different concentrations as shown in Fig. 16. The obtained cell viability was compared with control (cells without addition of sample) and which taken as 100%. As shown in Fig. 16, MTT assay was conducted to determine the viability of osteoblast-like MG 63 cell lines treated with different concentrations of nanohybrids and the obtained results indicates that nanohybrids did not show potent cell growth inhibitory effect on MG 63 cells. Specifically, different concentrations of CNTs-PAMAM(G3)-HAp induced merely less than 10% cell death even at 1000 μg/ml. Therefore, this experiment proved that nanohybrids do not induce any significant toxic property to osteoblast-like MG 63 cells. The more abundant of NH_2 groups present in PAMAM structure can easily form co-ordination bond with hydroxyapatite [31, 32]. Therefore, the abundant hydroxyapatite highly interacts with cell membrane and induces cells growth. In addition, to prove the non-toxic property of nanohybrids on osteoblast-like MG 63 cell, different concentration of nanohybrids were incubated. After incubation, morphological changes of osteoblast-like MG 63 cell were evaluated microscopically. Interestingly, MG 63 cell did not induce any cell death as shown in the representative optical microscopic images of CNTs-PAMAM(G3)-HAp nanohybrid (Fig. 17). Based on Fig. 17, it is observed that

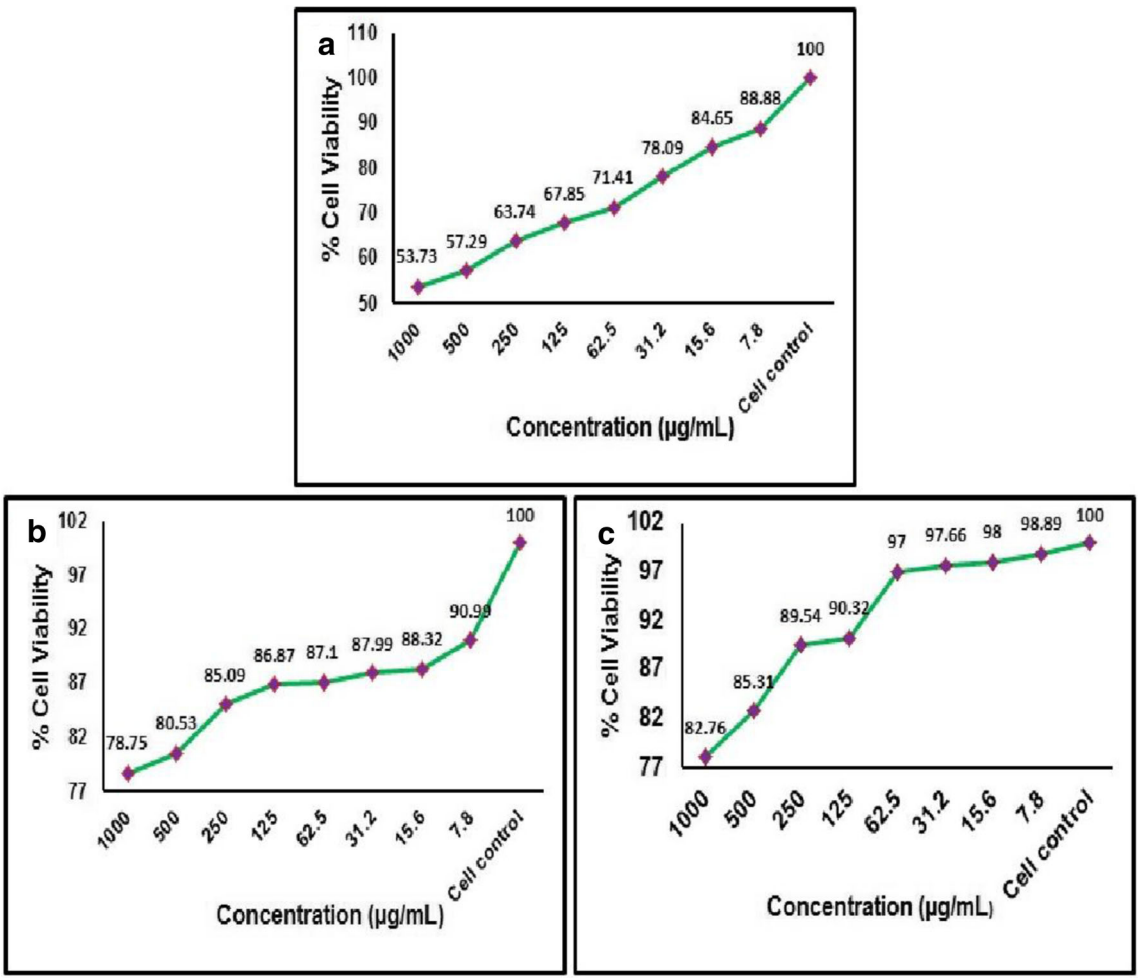

Fig. 16 MTT assay for (a) CNTs-PAMAM(G1)-HAp (b) CNTs-PAMAM(G2)-HAp and (c) CNTs-PAMAM(G3)-HAp on osteoblast-like MG 63 cells

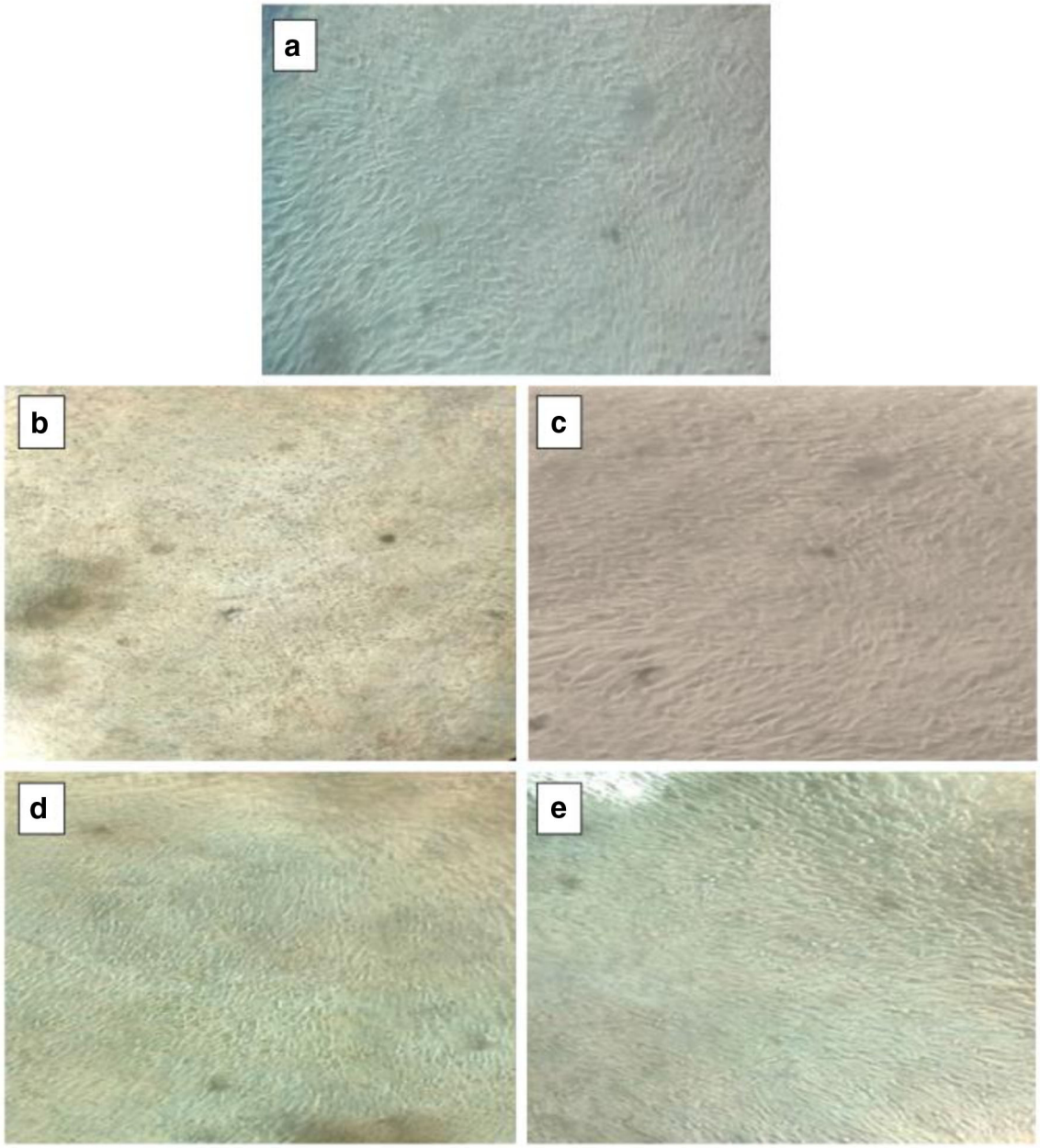

Fig. 17 Optical microscopy of CNTs-PAMAM(G3)-HAp on osteoblast-like MG 63 cells (a) control, (b) 1000 μg/mL, (c) 125 μg/mL, (d) 62.5 μg/mL and (e) 31.2 μg/mL

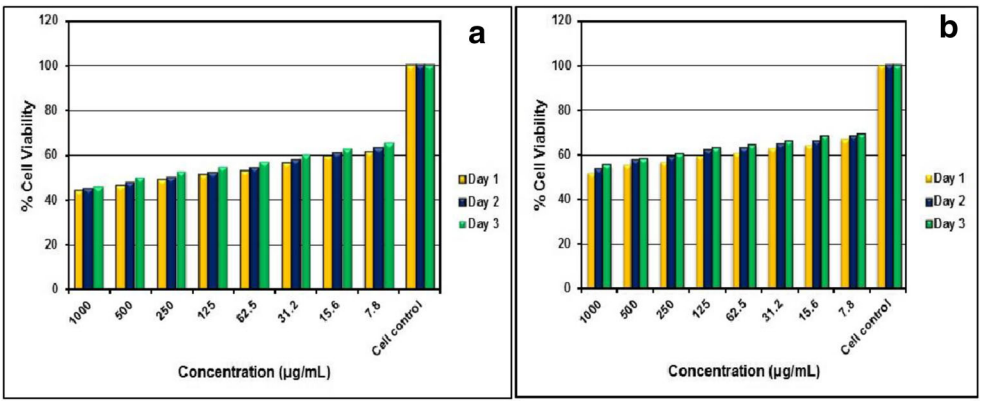

Fig. 18 MTT bar graph of (a) Pristine-CNTs and (b) nanostructured HAp

the nanohybrids are not induced any morphological changes or cell death on osteoblast-like MG 63 cells.

To verify the biocompatibility of the nanohybrids and their precursors (CNTs and HAp), the MTT cell viability assay was extended for three more days and the corresponding bar diagrams are shown in Figs. 18 and 19, respectively. The Pristine-MWCNTs (Fig. 18a) showed comparably low % of cell viability and which is due to the poor processability and dispersibility of CNTs with solvents [9]. Specifically, the high aspect ratio and strong van der Waals interactions between CNTs facilitate the lack of chemical affinity to aqueous and organic solvents and which produce poor reactivity with cell membrane. Even though, HAp resembles the inorganic component of bone, it exhibits low % of cell viability in Fig. 18b. Of course, HAp is highly biocompatible, biodegradable and osteoconductive material [3], but, the brittle nature and poor mechanical properties of inorganic bioactive materials cannot match with natural bone. Whereas, in Fig. 19, all the nanohybrids exhibit enhanced cell viability. Particularly, the nanohybrids derived from PAMAM(G3) matrix showed higher activity in cell growth than remaining hybrids and which was due to the fact that the Ca^{2+} ions located on the terminated surface of HAp crystals have coordination number seven, which are strictly held in the structure. Therefore, there is a possibility to form coordination bonds between the -NH_2 of PAMAM and Ca^{2+} of hydroxyapatite.

The biosafety of the materials (viz., CNTs, dendrimer and HAp) used in this research was confirmed with previous reports. There are wide varieties of research reported the clinical advantages of dendrimers such as safety, easy to handle and ease of mass production. For example, Pan Bifeng, et al., stated that the nanoparticles combined with dendrimer molecules can enhance the stability and dispersibility of the nanoparticles [5, 10, 14]. They have also reported that the combination of dendrimer and CNTs can suppress the cytotoxicity of CNTs and enhances the efficiency of the nanohybrids by facilitating the excellent physical, chemical and mechanical properties of CNTs to enter into the cytoplasm of the target cells. In addition, the average size of inorganic building blocks of bone was 20–40 nm, hence the synthesized hydroxyapatite with 20–40 nm size found in this research can enhance the biomineral formation [33]. Also, the nano-sized HAp showed greater activity in biomedical applications than larger-sized HAp particles [34]. Hence, the newly synthesized nanosize hydroxyapatite and its nanoeffects are also played a vital role to achieve a selective uptake and proliferation in osteoblast like MG 63 cells.

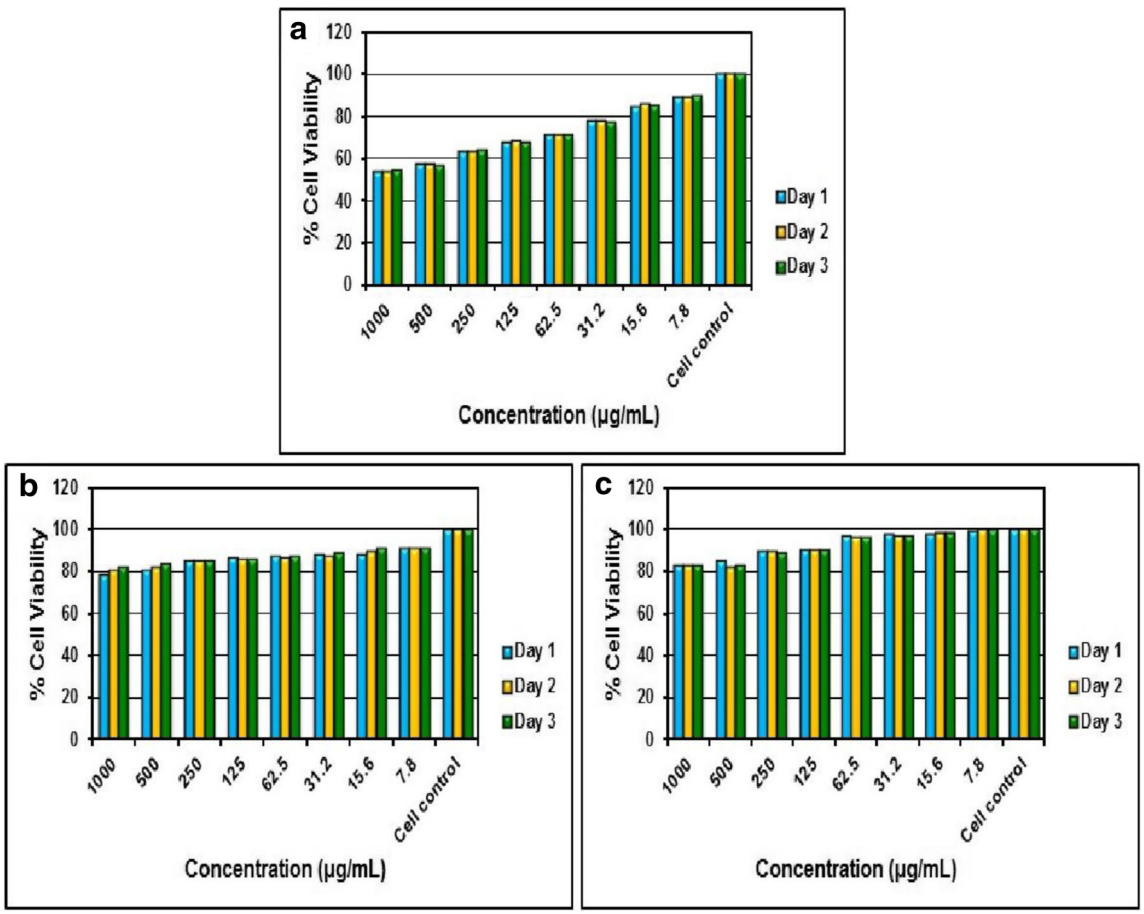

Fig. 19 MTT bar graph of (a) CNTs-PAMAM(G1)-HAp, (b) CNTs-PAMAM(G2)-HAp (c) CNTs-PAMAM(G3)-HAp on osteoblast-like MG 63 cells

Conclusion

Three different types of nanohybrids were synthesized by individual functionalization of PAMAM(G1), PAMAM(G2) and PAMAM(G3) dendrimers onto CNTs-COOH followed by the deposition of HAp. The structural and morphological behaviors of the obtained nanohybrids were investigated by spectroscopic and microscopic analyses. The in vitro cytotoxicity and cell proliferation was examined through osteoblast-like MG 63 cells using MTT assay. The dendrimer with higher generation number influences the cell proliferation and the order of reactivity was found as PAMAM(G3) > PAMAM(G2) > PAMAM(G1). The existence of more number of NH_2 groups in PAMAM(G3) can attract more number of HAp molecules onto their surface and the smaller size of the HAp particles facilities the cell growth even at higher concentration of nanohybrids applied for cell line studies. Hence the newly fabricated nanohybrids are promising candidates for bone tissue engineering applications in near future.

Acknowledgments Authors acknowledge Prof.E.Murugan for his valuable suggestions to carry out this work and the National Centre for Nanoscience and Nanotechnology (NCNSNT), University of Madras for providing financial support & instrumentation facilities.

References

1. De Witte TM, Fratila-Apachitei LE, Zadpoor AA, Peppas NA (2018) Bone tissue engineering via growth factor delivery: from scaffolds to complex matrices. Regenerative Biomaterials 5:197–211
2. Bapi G, Muktika T, Prashant K, Arun KI, Kiran K, Rakesh KT (2017) The use of nanoscaffolds and dendrimers in tissue engineering. Drug Discov Today 22:652–664
3. Merve H, Mehmet S (2017) Dendrimer functional hydroxyapatite nanoparticles generated by functionalization with siloxane-cored PAMAM dendrons. J Colloid Interface Sci 500:105–112
4. Molly MS (2008) Biomaterials for bone tissue engineering. Materialstoday 11:18–25
5. Pan B, Cui D, Xu P, Ozkan C, Feng G, Ozkan M, Huang T, Chu B, Li Q, He R, Hu G (2009) Synthesis and characterization of polyamidoamine dendrimer-coated multi-walled carbon nanotubes and their application in gene delivery systems. Nanotechnology 20: 125101
6. Viswanathan K, Periyannan K, Kasi G, Ayyakannu A, Marimuthu G, Naiyf SA, Jamal MK, Mohammed NA, Giovanni B (2018) Biocompatible properties of nano-drug carriers using TiO2-au embedded on multiwall carbon nanotubes for targeted drug delivery. Mater Sci Eng C 90:589–601
7. Bapi G, Hira C, Manisha P, Prashant K, Muhammad MA, Rakesh KT, Zahid H (2018) Carbon nanotube scaffolds as emerging nanoplatform for myocardial tissue regeneration: a review of recent developments and therapeutic implications. Biomed Pharmacother 104:496–508
8. Haniuh H, Saito N, Matsuda Y, Tsukahara T, Usui Y, Narita N, Hara K, Aoki K, Shimizu M, Ogihara N, Takanashi S, Okamoto M, Kobayashi S, Ishigaki N, Nakamura K, Kato H (2012) Basic potential of carbon nanotubes in tissue engineering applications. J Nanomater 2012:1–10
9. Massimo B, Lutz T, Huong H, Edvard M, Nunzio B, Marcia ID, Stefano B, Tomas M (2005) Covalent decoration of multi-walled carbon nanotubeswith silica nanoparticles. Chem Commun 14: 758–760
10. Pan B, Cui D, Gao F, He R (2006) Growth of multi-amine terminated poly(amidoamine) dendrimers on the surface of carbon nanotubes. Nanotechnology 17:2483–2489
11. Amirian M, Chakoli AN, Sui J, Cai W (2012) Enhanced shape memory effect of poly(L-lactide-co-ε-caprolactone) biodegradable copolymer reinforced with functionalized MWCNTs. J Polym Res 19(9777). https://doi.org/10.1007/s10965-011-9777-1
12. Zhang HL, Wang J, Yu N, Liu JS (2014) Electrospun PLGA/multi-walled carbon nanotubes/wool keratin composite membranes: morphological, mechanical, and thermal properties, and their bioactivities in vitro. J Polym Res 21(329). https://doi.org/10.1007/s10965-013-0329-8
13. El Sayed AM, Mohamad ADM (2018) Synthesis, structural, thermal, optical and dielectric properties of chitosan biopolymer; influence of PVP and α-Fe_2O_3 Nanorods. J Polym Res 25(175). https://doi.org/10.1007/s10965-018-1571-x
14. Pan B, Cui D, Sheng Y, Ozkan C, Gao F, Qing HR (2007) Li,1 Ping Xu, Huang T. Dendrimer-Modified Magnetic Nanoparticles Enhance Efficiency of Gene Delivery System Cancer Res 67: 8156–8163
15. Prashant K, Avinash G, Arun KI, Keerti J, Manish KC, Umesh G (2018) Dendrimer nanohybrid carrier systems: an expanding horizon for targeted drug and gene delivery. Drug Discov Today 23: 2300–314
16. Egambaram M, Sivaranjani A, Praba P (2016) New nanohybrids from poly(propylene imine) dendrimer stabilized silver nanoparticles on multiwalled carbon nanotubes for effective catalytic and antimicrobial applications. INT J POLYM MATER PO 65:111–124
17. Sivaranjani A (2017) New multi-walled carbon nanotubes functionalized with dendrimer stabilized palladium nanoparticles catalyst for C-C cross coupling reactions. Nanomater Mol Nanotechnol 6: 1–10. https://doi.org/10.4172/2324-8777.1000228
18. Eagambaram M, Sivaranjani A (2014) New dendrimer functionalized multi-walled carbon nanotube hybrids for bone tissue engineering. RSC Adv 4:35428–35441
19. Sivaranjani A, Padmapriya R, Lakshmi Devi C (2019) Synthesis and characterizations of biocompatible polymers and carbon nanotubes-based hybrids for biomedical applications. Int J Polym Mater Polym Biomater:1–12. https://doi.org/10.1080/00914037.2019.1616200
20. Preeti MB, Singh K (2018) In-situ fabrication of rod shaped nano-hydroxyapatite using microwave assisted semi-interpenetrating network as a template-morphology controlled approach. Mater Chem Phys 208:49–60
21. Markovic M, Fowler B, Tung M (2004) Preparation and comprehensive characterization of a calcium hydroxyapatite reference material. J Res Natl Inst Stand Technol 109:553–568
22. Thein-Han WW, Misra RDK (2009) Biomimetic chitosan-nanohydroxyapatite composite scaffolds for bone tissue engineering. Acta Biomater 5:1182–1197
23. Rao DV, Gigante GE, Cesareo R, Brunetti A, Schiavon N, Akatsuka T, Yuasa T, Takeda T (2017) Synchrotron-based XRD from rat bone of different age groups. Mater Sci Eng C 74:207–218
24. Kunio E (2003) Dendrimers for nanoparticle synthesis and dispersion stabilization. Top Curr Chem 227:31–52
25. Wenying L, Yi-Chun Y, Justin L (2011) Enhancing the stiffness of electrospun nanofiber scaffolds with a controlled surface coating and mineralization. Langmuir 27:9088–9093
26. Dahle S, Voigts F, Maus-Friedrichs W (2012) In situ preparation of calcium carbonate films. Thin Solid Films 520:1842–1846

27. Cai YL, Zhang S, Zeng XT (2011) Effect of fluorine incorporation on long-term stability of magnesium-containing hydroxyapatite coatings. J Mater Sci Mater Med 22:1633–1638
28. Dias AG, Skakle JMS, Gibson IR (2015) In situ thermal and structural characterization of bioactive calcium phosphate glass ceramics containing TiO2 and MgO oxides: high temperature - XRD studies. J Non-Cryst Solids 351:810–817
29. Zengjie F, Jinqing W, Zhaofeng W (2014) One-pot synthesis of graphene/hydroxyapatite nanorod composite for tissue engineering. Carbon 66:407–416
30. Mosmann T (1983) Rapid colorimetric assay for cellular growth and survival: application to proliferation and cytotoxicity assays. J Immunol Methods 65:55–63
31. Hossaing SF, Hubbell JA (1994) Molecular weight dependence of calcification of polyethylene glycol hydrogels. Biomaterials 15: 921–925
32. Kunneng L, He Y, Jianshu L, Jiaojiao Y, Xin Z, Libang H, Lei C, Yuan G, Xin X, Xuedong Z, Jiyao L (2015) Remineralization of demineralized dentin induced by amine-terminated PAMAM dendrimer. Macromol.Mater.Eng 300:107–117
33. Tang RK, Wang LJ, Orme CA, Bonstein T, Bush PJ, Nancollas GH (2004) Dissolution at the nanoscale: self-preservation of biominerals. Angew Chem Int Ed 43:2697–2701
34. Yurong C, Yukan L, Weiqi Y, Qinghong H, Jinhui T, Ming Z, Zhongli S, Ruikang T (2007) Role of hydroxyapatite nanoparticle size in bone cell proliferation. J Mater Chem 17:3780–3787